Condensed Matter Physics, 2001, Vol. 4, No. 3(27), pp. 553–578

CONDENSED MATTER PHYSICS

Influence of $\sigma_1 - \sigma_2$ stress on phase transition and physical properties of KD_2PO_4-type ferroelectrics

I.V.Stasyuk [1], R.R.Levitskii [1], I.R.Zachek [2], A.S.Duda [1]

[1] Institute for Condensed Matter Physics of the National Academy of Sciences of Ukraine, 1 Svientsitskii Str., 79011 Lviv, Ukraine

[2] State University “Lvivska Politekhnika”, 12 Bandera Str., 79013 Lviv, Ukraine

Received June 20, 2001

Within the proposed earlier model we study effects of stress $\sigma_1 - \sigma_2$ on the KD_2PO_4 type ferroelectrics. In the cluster approximation for the short-range correlations, we calculate dielectric, piezoelectric, and elastic characteristics of a strained by $\sigma_1 - \sigma_2$ KD_2PO_4 type crystal. Numerical analysis of the obtained results is performed. Stress dependences of the calculated characteristics and the phase diagram are explored. Possibility of the induced by $\sigma_1 - \sigma_2$ phase transition into a new paraelectric phase with monoclinic symmetry is discussed.

PACS: *77.80.-e, 77.80.Bh, 77.84.Fa*

Key words: *shear stress, monoclinic phase, phase diagram, piezoelectricity, strain, KDP*

1. Introduction

Pressures that do not lower the symmetry of the KH_2PO_4 family ferroelectrics (hydrostatic and uniaxial $p = -\sigma_3$) only lower the transition temperature in these crystals. In contrast, the shear stresses of different symmetries can produce qualitative changes in the phase diagrams, inducing new phase transitions or removing the existing ones. Thus the shear stress $\sigma_{xy} = \sigma_6$, which in these crystals is an external field conjugate to the order parameter, smears out the ferroelectric phase transition, reducing the jump of polarization until it entirely vanishes at a certain critical stress [1,2].

External pressure studies of the KH_2PO_4 family systems in our group were initiated by Stasyuk and Biletskii in [3,4] where they proposed a microscopic model of strained KD_2PO_4. They established a form of the internal fields and splittings of the deuteron short-range configuration energies produced by piezoelectric and strictional coupling with lattice strains of different symmetries, as well as by mere changes in the interparticle distances. Within this approach we later studied hydrostatic and uniaxial σ_3 pressures effects in the KH_2PO_4 family crystals, developing a unified model for both ferroelectric and antiferroelectric systems of this type [5] and revealing a universal dependence of the transition temperature in several crystals of this family on the distance between the equilibrium hydrogen sites on bond.

In [3,4] Stasyuk and Biletskii also explored the effects of the $\sigma_1 - \sigma_2$ ($\sigma_{xx} - \sigma_{yy}$) stress on the phase diagram of a KD_2PO_4 crystal. This symmetrized stress is transformed via the B_1 irreducible representation and is a purely shear stress in the paraelectric phase. Its practical realization (simultaneous compression along the axis a and stretching along the axis b) is a rather complicated task; however, it is interesting from a theoretical standpoint in connection with the fact that highly deuterated KD_2PO_4 and RbD_2PO_4 easier crystallize in a monoclinic modification rather than in a usual tetragonal one. It has been shown [3,4] that high enough values of the $\sigma_1 - \sigma_2$ stress induce a phase transition into a new phase, of presumably monoclinic symmetry with the strain $\varepsilon_1 - \varepsilon_2$ significantly larger than at stresses right below the critical one. This indicates that monoclinic lattice symmetry of highly deuterated KD_2PO_4 and RbD_2PO_4 might result from local stresses $\sigma_1 - \sigma_2$ produced by inclusion of larger ions.

In the present paper we return to the studies of the $\sigma_1 - \sigma_2$ stress and explore its influence on the phase diagram, dielectric, piezoelectric, and elastic properties of the KD_2PO_4 type crystals.

2. Thermodynamics. The four-particle cluster approximation

We consider a system of deuterons moving on the hydrogen bonds O–D. . . O in a ferroelectric KD_2PO_4 type crystal. A primitive cell of the crystal consists of two neighbouring tetrahedra PO_4 along with four hydrogen bonds attached to one of them (type "A" tetrahedra). The bonds attached to the other tetrahedron (of the "B" type) belong to the four nearest structural elements surrounding it.

To a crystal we apply a stress $\sigma_1 - \sigma_2 \equiv \sigma_{12}$. If $\sigma_1 = \sigma_2$, in the paraelectric phase only two components of the strain tensor are different from zero: ε_1 and ε_2, and $\varepsilon_1 = -\varepsilon_2$. In the ferroelectric phase due to the difference in the elastic constants $c_{11}^E \neq c_{22}^E$ the strains ε_1 and $-\varepsilon_2$ may differ as well, but slightly. Therefore, in the microscopic Hamiltonian below we take into account only the contributions of a symmetrized strain $\varepsilon_{12} \equiv \varepsilon_1 - \varepsilon_2$ and neglect all the effects related to $\varepsilon_1 + \varepsilon_2$; however, we separate ε_1 and ε_2 when necessary.

Hamiltonian of a deuteron subsystem of the KD_2PO_4 crystal, to which the shear stress $\sigma_1 - \sigma_2 \equiv \sigma_{12}$ and electric fields E_i ($i = 1, 2, 3$) are applied, reads [3,4]:

$$\hat{H}_i = \frac{\bar{v}N}{2}(c_{11}^{0E}\varepsilon_1^2 + 2c_{12}^{0E}\varepsilon_1\varepsilon_2 + c_{22}^{0E}\varepsilon_2^2) - \frac{\bar{v}N}{2}\chi_{33}^0 E_3^2$$

$$
\begin{aligned}
&+\sum_{\substack{q_1q_2\\q_3q_4}}\left\{\frac{1}{2}\sum_{ff'}V_{ff'}\frac{\sigma_{q_ff}}{2}\frac{\sigma_{q_{f'}f'}}{2}+\Phi\frac{\sigma_{q_11}}{2}\frac{\sigma_{q_22}}{2}\frac{\sigma_{q_33}}{2}\frac{\sigma_{q_44}}{2}\right\}\\
&\times\{\delta_{q_1q_2}\delta_{q_1q_3}\delta_{q_1q_4}+\delta_{q_1+r_2,q_2}\delta_{q_1+r_3,q_3}\delta_{q_1+r_4,q_4}\}\\
&+\frac{1}{2}\sum_{\substack{aa'\\ff'}}J_{ff'}(qq')\frac{\sigma_{q_ff}}{2}\frac{\sigma_{q_{f'}f'}}{2}-\sum_{qf}[2\mu F^i_f(12)+\mu_{f_i}E_i]\;\frac{\sigma_{qf}}{2}.
\end{aligned}
\tag{2.1}
$$

Two first terms in the Hamiltonian correspond to the elastic and electric energies stored in a crystal and independent of the deuteron subsystem configuration; c_{ij}^{0E} and χ_{33}^0 are the "seed" elastic constants and dielectric susceptibility; $\bar{v}=v/k_{\mathrm{B}}$ is the primitive cell volume normalized per Boltzmann constant k_{B}.

The third and the fourth terms in the Hamiltonian describe configurational short-range interactions between deuterons surrounding tetrahedra of the "A" and "B" types (first and second products of the δ-functions, respectively). The eigenvalues of the operator $\sigma_{qf}=\pm1$ correspond to two equilibrium deuteron sites on the fth bond in the qth unit cell. $J_{ff'}(qq')$ are the constants of the long-range interactions (dipole-dipole and lattice mediated) between deuterons.

Factors $\mu F^i_f(12)$ are internal fields created by strictional coupling with the strains ε_1 and ε_2 [3,4]

$$
\mu F^i_f(12)=\sum_{f'}\psi_{ff'}\langle\sigma_{qf'}\rangle\varepsilon_i. \tag{2.2}
$$

Symmetry analysis of the above fields have been performed in [3,4].

In an unstrained crystal there is a single order parameter

$$
\eta^{(1)}=\langle\sigma_{q1}\rangle=\langle\sigma_{q2}\rangle=\langle\sigma_{q3}\rangle=\langle\sigma_{q4}\rangle. \tag{2.3}
$$

An external stress σ_{12} breaks equivalence of hydrogen bonds. It shortens the bonds going along the a-axis and elongates those going along the b-axis. The deuteron ordering is then characterized by two order parameters

$$
\eta^{(1)}_{13}=\langle\sigma_{q1}\rangle=\langle\sigma_{q3}\rangle,\quad \eta^{(1)}_{24}=\langle\sigma_{q2}\rangle=\langle\sigma_{q4}\rangle. \tag{2.4}
$$

Static and dynamic properties of the KD_2PO_4 type crystals will be considered in the four-particle cluster approximation with the Hamiltonian H_4^{iA}:

$$
\begin{aligned}
&\hat{H}_4^{iA}=\sum_q\hat{H}^{iA}_{4q}\;=\\
&=\sum_q\Big\{V\;\left(\frac{\sigma_{q1}}{2}\frac{\sigma_{q2}}{2}+\frac{\sigma_{q2}}{2}\frac{\sigma_{q3}}{2}+\frac{\sigma_{q3}}{2}\frac{\sigma_{q4}}{2}+\frac{\sigma_{q4}}{2}\frac{\sigma_{q1}}{2}\right)+\\
&+(U+2\delta_{12}\;\varepsilon_{12})\;\frac{\sigma_{q1}}{2}\frac{\sigma_{q3}}{2}+(U-2\delta_{12}\varepsilon_{12})\frac{\sigma_{q2}}{2}\frac{\sigma_{q4}}{2}+\Phi\frac{\sigma_{q1}}{2}\frac{\sigma_{q2}}{2}\frac{\sigma_{q3}}{2}\frac{\sigma_{q4}}{2}-\hat{H}^i_4(q)\Big\},
\end{aligned}
\tag{2.5}
$$

$$
\hat{H}_4^z(q)=\frac{z^z_{13}}{\beta}\Big(\frac{\sigma_{q1}}{2}+\frac{\sigma_{q3}}{2}\Big)+\frac{z^z_{24}}{\beta}\Big(\frac{\sigma_{q2}}{2}+\frac{\sigma_{q4}}{2}\Big)\;,
$$

$$\hat{H}_4^x(q) = \frac{z_1^x}{\beta}\frac{\sigma_{q1}}{2} + \frac{z_3^x}{\beta}\frac{\sigma_{q3}}{2} + \frac{z_{24}^x}{\beta}\left(\frac{\sigma_{q2}}{2} + \frac{\sigma_{q4}}{2}\right),$$
$$\hat{H}_4^y(q) = \frac{z_3^y}{\beta}\left(\frac{\sigma_{q1}}{2} + \frac{\sigma_{q3}}{2}\right) + \frac{z_2^y}{\beta}\frac{\sigma_{q2}}{2} + \frac{z_4^y}{\beta}\frac{\sigma_{q4}}{2}, \tag{2.6}$$

where

$$V = -\frac{w_1}{2}, \quad U = -\varepsilon + \frac{w_1}{2}, \quad \Phi = 4\varepsilon - 8w + 2w_1,$$

and ε, ω, ω_1 are the energies of short-range deuteron configurations. The induced by the stress σ_{12} strain ε_{12} lowers the system symmetry and splits the energy levels of the single-ionized (one- and three-particle) deuteron configurations to two levels with the energies [3,4]

$$w^{\pm} = w \pm \delta_{12}\varepsilon_{12}, \tag{2.7}$$

with the splitting constant δ_{12}. Energies of the other short-range energy levels remain unchanged [3,4].

The effective fields z_f^i have the following symmetry

$$\begin{aligned}
z_{13}^z &= \beta\ [-\Delta_{13} + (\nu + \bar{\nu} + 2\psi_2\varepsilon_{12})\ \eta_{13}^{(1)z} + (\nu - \bar{\nu})\eta_{24}^{(1)z} + \mu_3 E_3],\\
z_{24}^z &= \beta\ [-\Delta_{24} + (\nu - \bar{\nu})\eta_{13}^{(1)z} + (\nu + \bar{\nu} - 2\psi_2\varepsilon_{12})\eta_{24}^{(1)z} + \mu_3 E_3];\\
z_1^x &= \beta\ [-\Delta_1 + 2(\nu_1 + \psi_1\varepsilon_{12})\ \eta_1^{(1)x} + 2(\nu_3 + \psi_3\varepsilon_{12})\eta_3^{(1)x} + 4\nu_2\eta_{24}^{(1)x} + \mu_1 E_1],\\
z_3^x &= \beta\ [-\Delta_3 + 2(\nu_3 + \psi_3\varepsilon_{12})\ \eta_1^{(1)x} + 2(\nu_1 + \psi_1\varepsilon_{12})\eta_3^{(1)x} + 4\nu_2\eta_{24}^{(1)x} - \mu_1 E_1],\\
z_{24}^x &= \beta[-\Delta_{24} + 2\nu_2(\eta_1^{(1)x} + \eta_3^{(1)x}) + 2(\nu_1 + \nu_3 - \psi_2\varepsilon_{12})\eta_{24}^{(1)x}];\\
z_{13}^y &= \beta[-\Delta_{13} + 2(\nu_1 + \nu_3 + \psi_2\varepsilon_{12})\eta_{13}^{(1)y} + 2\nu_2(\eta_2^{(1)y} + \eta_4^{(1)y})],\\
z_2^y &= \beta[-\Delta_2 + 4\nu_2\eta_{13}^{(1)y} + 2(\nu_1 - \psi_1\varepsilon_{12})\eta_2^{(1)y} + 2(\nu_3 - \psi_3\varepsilon_{12})\eta_4^{(1)y} - \mu_2 E_2],\\
z_4^y &= \beta[-\Delta_4 + 4\nu_2\eta_{13}^{(1)y} + 2(\nu_3 - \psi_3\varepsilon_{12})\eta_2^{(1)y} + 2(\nu_1 - \psi_1\varepsilon_{12})\eta_4^{(1)y} + \mu_2 E_2],
\end{aligned} \tag{2.8}$$

where

$$\begin{aligned}
&\nu_1 = \frac{J_{11}}{4}, \quad \nu_2 = \frac{J_{12}}{4}, \quad \nu_3 = \frac{J_{13}}{4},\\
&\nu = \nu_1 + 2\nu_2 + \nu_3, \quad \bar{\nu} = \nu_1 - 2\nu_2 + \nu_3, \quad \psi_2 = \psi_1 + \psi_3\\
&\mu_3 = \mu_{13} = \mu_{23} = \mu_{33} = \mu_{43},\\
&\mu_1 = \mu_{11} = -\mu_{31}, \ \mu_{21} = \mu_{41} = 0,\\
&\mu_2 = \mu_{22} = -\mu_{42}, \ \mu_{12} = \mu_{32} = 0,
\end{aligned}$$

ψ_1, ψ_3 are the so-called deformation potentials.

The single-particle deuteron Hamiltonians under the stress σ_{12} and in the field E_i read

$$\begin{aligned}
\hat{H}_{1,3}^{(1)z} &= -\frac{\bar{z}_{13}^z}{\beta}\frac{\sigma_{q1,3}}{2}, \quad \hat{H}_{2,4}^{(1)z} = -\frac{\bar{z}_{24}^z}{\beta}\frac{\sigma_{q2,4}}{2};\\
\hat{H}_{1,3}^{(1)x} &= -\frac{\bar{z}_{1,3}^x}{2}\frac{\sigma_{q1,3}}{2}, \quad \hat{H}_{2,4}^{(1)x} = -\frac{\bar{z}_{24}^x}{\beta}\frac{\sigma_{q2,4}}{2};\\
\hat{H}_{1,3}^{(1)y} &= -\frac{\bar{z}_{13}^y}{2}\frac{\sigma_{q1,3}}{2}, \quad \hat{H}_{2,4}^{(1)y} = -\frac{\bar{z}_{2,4}^y}{\beta}\frac{\sigma_{q2,4}}{2}.
\end{aligned} \tag{2.9}$$

The expressions for $\bar{z}^z_{13}, ..., \bar{z}^y_{2,4}$ can be obtained from (2.8) by changing $\Delta_{13}, ..., \Delta_4$ with $2\Delta_{13}, ..., 2\Delta_4$.

The single-particle distribution functions calculated within the four-particle cluster approximation are

$$\eta^{(1)z}_{13} = \frac{m^z_{13}}{D^z_{12}}; \qquad \eta^{(1)z}_{24} = \frac{m^z_{24}}{D^z_{12}}, \tag{2.10}$$
$$\eta^{(1)x}_{\substack{1\\3}} = \frac{m^x_{\substack{1\\3}}}{D^x_{12}}, \quad \eta^{(1)x}_{24} = \frac{m^x_{24}}{D^x_{12}}; \quad \eta^{(1)y}_{13} = \frac{m^y_{13}}{D^y_{12}}, \quad \eta^{(1)y}_{\substack{2\\4}} = \frac{m^y_{\substack{2\\4}}}{D^y_{12}},$$

where the following notations are used

$$\begin{aligned}
m^z_{13} &= \sinh(z^z_{13} + z^z_{24}) + d\sinh(z^z_{13} - z^z_{24}) + 2bc_{12}\sinh z^z_{13},\\
m^z_{24} &= \sinh(z^z_{13} + z^z_{24}) - d\sinh(z^z_{13} - z^z_{24}) + 2\frac{b}{c_{12}}\sinh z^z_{24},\\
m^x_{\substack{1\\3}} &= \sinh A^x_1 + d\sinh A^x_2 \pm 2a\sinh A^x_3\\
&\quad \pm \frac{b}{c_{12}}\sinh A^x_5 \pm \frac{b}{c_{12}}\sinh A^x_6 + 2bc_{12}\sinh A^x_7),\\
m^x_{24} &= \sinh A^x_1 - d\sinh A^x_2 + \frac{b}{c_{12}}(\sinh A^x_5 - \frac{b}{c_{12}}\sinh A^x_6,\\
m^y_{13} &= \sinh B^y_1 - d\sinh B^y_2 + bc_{12}\sinh B^y_7 + bc_{12}\sinh B^y_8,\\
m^y_{\substack{2\\4}} &= \sinh B^y_1 + d\sinh B^y_2 \pm 2a\sinh B^y_4 + 2\frac{b}{c_{12}}\sinh B^y_6\\
&\pm bc_{12}\sinh B^y_7 \mp bc_{12}\sinh B^y_8.
\end{aligned} \tag{2.11}$$

$$\begin{aligned}
D^z_{12} &= \cosh(z^z_{13} + z^z_{24}) + d\cosh(z^z_{13} - z^z_{24}) + 2a + 2bc_{12}\cosh z^z_{13} + 2\frac{b}{c_{12}}\cosh z^z_{24},\\
D^x_{12} &= \cosh A^x_1 + d\cosh A^x_2 + 2a\cosh A^x_3 + 2\frac{b}{c_{12}}\cosh A^x_5 + 2bc_{12}\cosh A^x_7,\\
D^y_{12} &= \cosh B^y_1 + d\cosh B^y_2 + 2a\cosh B^y_4 + 2\frac{b}{c_{12}}\cosh B^y_6 + 2bc_{12}\cosh B^y_8,
\end{aligned}$$

and

$$\begin{aligned}
&A^x_{\substack{1\\2}} = 2(z^x_1 + z^x_3 \pm 2z^x_{24}), \quad A^x_3 = 2(z^x_1 - z^x_3),\\
&A^x_{\substack{5\\6}} = 2(z^x_1 - z^x_3 \pm 2z^x_{24}), \quad A^x_7 = 2(z^x_1 + z^x_3),\\
&B^y_{\substack{1\\2}} = 2(z^y_{13} \pm z^y_2 \pm z^y_4), \quad B^y_4 = 2(z^y_2 - z^y_4),\\
&B^y_6 = 2(z^y_2 + z^y_4), \quad B^y_{\substack{7\\8}} = 2(2z^y_{13} \pm z^y_2 \mp z^y_4),\\
&a = \exp(-\beta\varepsilon), \quad b = \exp(-\beta w),\\
&d = \exp(-\beta w_1), \quad c_{12} = \exp(-\beta\delta\varepsilon_{12}).
\end{aligned} \tag{2.12}$$

After excluding $\Delta_{13}, ..., \Delta_4$ from (2.8), the quantities $z_{13}^z, ..., z_4^y$ acquire the form

$$
\begin{aligned}
z_{13}^z &= \frac{1}{2}\ln\,\frac{1+\eta_{13}^{(1)}}{1-\eta_{13}^{(1)}} + \frac{\beta}{2}\left[(\nu+\bar\nu+\psi_2\varepsilon_{12})\eta_{13}^{(1)z} + (\nu-\bar\nu)\eta_{24}^{(1)z} + \mu_3 E_3\right],\\
z_{24}^z &= \frac{1}{2}\ln\,\frac{1+\eta_{24}^{(1)}}{1-\eta_{24}^{(1)}} + \frac{\beta}{2}\left[(\nu-\bar\nu)\eta_{13}^{(1)z} + (\nu+\bar\nu-\psi_2\varepsilon_{12})\eta_{24}^{(1)z} + \mu_3 E_3\right],\\
z_{\frac{1}{3}}^x &= \frac{1}{2}\ln\,\frac{1+\eta_{\frac{1}{3}}^{(1)x}}{1-\eta_{\frac{1}{3}}^{(1)x}} + \beta(\nu_{\frac{1}{3}}+\psi_{\frac{1}{3}}\varepsilon_{12})\eta_1^{(1)x} + \beta(\nu_{\frac{1}{3}}+\psi_{\frac{1}{3}}\varepsilon_{12})\eta_3^{(1)x}\\
&\quad + 2\beta\nu_2\;\eta_{24}^{(1)x} \pm \frac{\beta}{2}\mu_1 E_1,\\
z_{24}^x &= \frac{1}{2}\ln\,\frac{1+\eta_{24}^{(1)}x}{1-\eta_{24}^{(1)x}} + \beta\nu_2(\eta_1^{(1)x}+\eta_3^{(1)x}) + \beta(\nu_1+\nu_3-\psi_2\varepsilon_{12})\eta_{24}^{(1)x},\\
z_{13}^y &= \frac{1}{2}\ln\,\frac{1+\eta_{13}^{(1)}y}{1-\eta_{13}^{(1)y}} + \beta(\nu_1+\nu_3+\psi_2\varepsilon_{12})\eta_{13}^{(1)y} + \beta\nu_2(\eta_2^{(1)x}+\eta_4^{(1)x}),\\
z_{\frac{2}{4}}^y &= \frac{1}{2}\ln\,\frac{1+\eta_{\frac{2}{4}}^{(1)y}}{1-\eta_{\frac{2}{4}}^{(1)y}} + 2\beta\nu_2\eta_{13}^{(1)y} + \beta(\nu_{\frac{1}{3}}-\psi_{\frac{1}{3}}\varepsilon_{12})\eta_2^{(1)y}\\
&\quad + \beta(\nu_{\frac{1}{3}}-\psi_{\frac{1}{3}}\varepsilon_{12})\eta_4^{(1)y} \pm \frac{\beta}{2}\mu_2 E_2.
\end{aligned}
$$

Finally, we calculate the thermodynamic potential of a deuteron subsystem of the KD_2PO_4 type crystal to which the stress σ_{12} is applied. In the used four-particle cluster approximation we obtain

$$
\begin{aligned}
&g_{1E}(12) = \frac{1}{2}\bar v(c_{11}^{0E}\varepsilon_1^2 + 2c_{12}^{0E}\varepsilon_1\varepsilon_2 + c_{22}^{0E}\varepsilon_2^2) - \frac{\bar v}{2}\chi_{33}^0 E_3^2 + 2T\ln 2\\
&+\frac{1}{2}(\nu+\bar\nu)\left[\left(\eta_{13}^{(1)z}\right)^2 + \left(\eta_{24}^{(1)z}\right)^2\right] + (\nu-\bar\nu)\eta_{13}^{(1)z}\eta_{24}^{(1)z} + \psi_{12}\varepsilon_{12}\left[\left(\eta_{13}^{(1)z}\right)^2 - \left(\eta_{24}^{(1)z}\right)^2\right]\\
&-T\ln\left[1-\left(\eta_{13}^{(1)z}\right)^2\right]\left[1-\left(\eta_{24}^{(1)z}\right)^2\right] - 2T\ln D^z - \bar v(\sigma_1\varepsilon_1+\sigma_2\varepsilon_2). \qquad (2.13)
\end{aligned}
$$

Thermodynamic equilibrium conditions are

$$
\begin{aligned}
&\frac{1}{\bar v}\left(\frac{\partial g_{1E}(12)}{\partial\varepsilon_1}\right)_{E_3,\sigma_{12}} = 0, \quad \frac{1}{\bar v}\left(\frac{\partial g_{1E}(12)}{\partial\varepsilon_2}\right)_{E_3,\sigma_{12}} = 0,\\
&\frac{1}{\bar v}\left(\frac{\partial g_{1E}(12)}{\partial E_3}\right)_{\varepsilon_{12},\sigma_{12}} = -P_3. \qquad (2.14)
\end{aligned}
$$

Using (2.13) and (2.14) we obtain

$$
\sigma_1 = (c_{11}^{0E}\varepsilon_1 + c_{12}^{0E}\varepsilon_2) - \frac{\psi_{12}}{\bar v}\left[(\eta_{13}^{(1)z})^2 - (\eta_{24}^{(1)z})^2\right]
$$

$$
\begin{aligned}
&+\frac{2\delta_{12}}{\bar{v}D^z_{12}}\left(2bc_{12}\cosh z^z_{13} - 2\frac{b}{c_{12}}\cosh z^z_{24}\right),\\
\sigma_2 &= (c^{0E}_{12}\varepsilon_1 + c^{0E}_{22}\varepsilon_2) + \frac{\psi_{12}}{\bar{v}}\left[(\eta^{(1)z}_{13})^2 - (\eta^{(1)z}_{24})^2\right]\\
&-\frac{2\delta_{12}}{\bar{v}D^z_{12}}\left(2bc_{12}\cosh z^z_{13} - 2\frac{b}{c_{12}}\cosh z^z_{24}\right),
\end{aligned} \tag{2.15}
$$

$$
P_3 = \chi^0_{33}E_3 + \frac{\mu_{13}}{\bar{v}}\frac{m^z_{13}}{D^z_{12}} + \frac{\mu_{24}}{\bar{v}}\frac{m^z_{24}}{D^z_{12}}. \tag{2.16}
$$

From (2.16) the electric field

$$
E_3 = \frac{1}{\chi^0_{33}}P_3 - \frac{1}{\chi^0_{33}}\left(\frac{\mu_{13}}{v}\frac{m^z_{13}}{D^z_{12}} + \frac{\mu_{24}}{v}\frac{m^z_{24}}{D^z_{12}}\right). \tag{2.17}
$$

Hence, the system of equations for $\eta^{(1)}_{13}$, $\eta^{(1)}_{24}$, and ε_{12} can be written as

$$
\begin{aligned}
&\eta^{(1)}_{13} = \frac{m_{13}}{D_{12}}, \quad \eta^{(1)}_{24} = \frac{m_{24}}{D_{12}},\\
&\sigma_1 - \sigma_2 = (c^0_{11} - c^0_{12})\varepsilon_1 - (c^0_{22} - c^0_{12})\varepsilon_2\\
&-\frac{2\psi_{12}}{\bar{v}}\left[(\eta^{(1)}_{13})^2 - (\eta^{(1)}_{24})^2\right] - \frac{4\delta_{12}}{\bar{v}D_{12}}\left(2bc_{12}\cosh z_{13} - 2\frac{b}{c_{12}}\cosh z_{24}\right).
\end{aligned} \tag{2.18}
$$

In the paraelectric phase the following relation between σ_{12} and ε_{12} holds

$$
\sigma_{12} = (c^0_{11} - c^0_{12})\varepsilon_{12} - \frac{16\delta_{12}b\sinh\beta\delta_{12}\varepsilon_{12}}{\bar{v}(1 + 2a + 2d + 4b\cosh\beta\delta_{12}\varepsilon_{12}}. \tag{2.19}
$$

The first order phase transition temperature between the ferroelectric and paraelectric phases T_c is obtained from the following system of equations

$$
\begin{aligned}
&g_{1E}[\eta^{(1)}_{13}(T_\mathrm{c}), \eta^{(1)}_{24}(T_\mathrm{c}), \varepsilon_{12}, T_\mathrm{c}] = g_{1E}(0, 0, \varepsilon_{12}, T_\mathrm{c}),\\
&\eta^{(1)}_{13}(T_\mathrm{c}) = \frac{m_{13}(T_\mathrm{c})}{D_{12}(T_\mathrm{c})},\\
&\eta^{(1)}_{24}(T_\mathrm{c}) = \frac{m_{24}(T_\mathrm{c})}{D_{12}(T_\mathrm{c})}.
\end{aligned} \tag{2.20}
$$

3. Piezoelectric, elastic, and dielectric characteristics of KD_2PO_4 type crystals under the σ_{12} stress

The coefficients of piezoelectric stress are

$$
\begin{aligned}
e_{31} &= \left(\frac{\partial P_3}{\partial \varepsilon_1}\right)_{E_3} = \frac{\mu_{13}}{v}\left(\frac{\partial \eta^{(1)}_{13}}{\partial \varepsilon_1}\right)_{E_3} + \frac{\mu_{24}}{v}\left(\frac{\partial \eta^{(1)}_{24}}{\partial \varepsilon_1}\right)_{E_3},\\
e_{32} &= \left(\frac{\partial P_3}{\partial \varepsilon_2}\right)_{E_3} = \frac{\mu_{13}}{v}\left(\frac{\partial \eta^{(1)}_{13}}{\partial \varepsilon_2}\right)_{E_3} + \frac{\mu_{24}}{v}\left(\frac{\partial \eta^{(1)}_{24}}{\partial \varepsilon_2}\right)_{E_3}.
\end{aligned} \tag{3.1}
$$

Here we neglect stress and temperature dependences of the effective dipole moments μ_{13} and μ_{24}. From the expressions for the single-particle distribution functions (2.10), we obtain the following system of equations

$$N_{11}\left(\frac{\partial\eta_{13}^{(1)}}{\partial\varepsilon_1}\right)_{E_3}+N_{12}\left(\frac{\partial\eta_{24}^{(1)}}{\partial\varepsilon_1}\right)_{E_3}=N_1^{\varepsilon},$$
$$N_{21}\left(\frac{\partial\eta_{13}^{(1)}}{\partial\varepsilon_1}\right)_{E_3}+N_{22}\left(\frac{\partial\eta_{24}^{(1)}}{\partial\varepsilon_1}\right)_{E_3}=N_2^{\varepsilon}, \tag{3.2}$$

where

$$\begin{aligned}
&N_{11}=D-(\varphi_{13}^{\eta}\varkappa_{13}+\varphi_{1-4}^{\eta}s), \qquad N_{12}=-(\varphi_{1-4}^{\eta}\varkappa_{13}+\varphi_{24}^{\eta}s),\\
&N_{21}=-(\varphi_{13}^{\eta}s+\varphi_{1-4}^{\eta}\varkappa_{24}), \qquad N_{22}=D-(\varphi_{1-4}^{\eta}s+\varphi_{24}^{\eta}\varkappa_{24}),\\
&N_1^{\varepsilon}=\beta\theta_{13}, \qquad N_2^{\varepsilon}=\beta\theta_{24},
\end{aligned} \tag{3.3}$$

and

$$\begin{aligned}
&\theta_{13}=\psi_{12}\Big(\eta_{13}^{(1)}\varkappa_{13}-\eta_{24}^{(1)}s\Big)+\delta_{12}t_{13},\\
&\theta_{24}=\psi_{12}\Big(\eta_{13}^{(1)}s-\eta_{24}^{(1)}\varkappa_{24}\Big)+\delta_{12}t_{24},
\end{aligned} \tag{3.4}$$

$$\begin{aligned}
&\varkappa_{13}=\cosh(z_{13}+z_{24})+d\cosh(z_{13}-z_{24})+2bc_{12}\cosh z_{13}-\eta_{13}^{(1)}m_{13},\\
&\varkappa_{24}=\cosh(z_{13}+z_{24})+d\cosh(z_{13}-z_{24})+2\frac{b}{c_{12}}\cosh z_{24}-\eta_{24}^{(1)}m_{24},\\
&s=\cosh(z_{13}+z_{24})-d\cosh(z_{13}-z_{24})-\eta_{13}^{(1)}m_{24},\\
&t_{13}=-2bc_{12}\sinh z_{13}+\eta_{13}^{(1)}(2bc_{12}\cosh z_{13}-2\frac{b}{c_{12}}\cosh z_{24}),\\
&t_{24}=-2\frac{b}{c_{12}}\sinh z_{24}+\eta_{24}^{(1)}(2bc_{12}\cosh z_{13}-2\frac{b}{c_{12}}\cosh z_{24}),\\
&\varphi_{13}^{\eta}=\frac{1}{1-\eta_{13}^{(1)2}}+\frac{1}{2T}(\nu+\bar{\nu})+\frac{1}{T}\psi_{12}\varepsilon_{12},\\
&\varphi_{24}^{\eta}=\frac{1}{1-\eta_{24}^{(1)2}}+\frac{1}{2T}(\nu+\bar{\nu})-\frac{1}{T}\psi_{12}\varepsilon_{12},\\
&\varphi_{1-4}^{\eta}=\frac{1}{2T}(\nu-\bar{\nu}).
\end{aligned} \tag{3.5}$$

From the system (3.2), we obtain

$$\begin{aligned}
e_{31}=&\frac{\mu_{13}}{v}\frac{\beta}{\Delta}\{D\theta_{13}+\varphi_{24}^{\eta}(-\theta_{13}\varkappa_{24}+\theta_{24}s)+\varphi_{1-4}^{\eta}(-\theta_{13}s+\theta_{24}\varkappa_{13})\}\\
&+\frac{\mu_{24}}{v}\frac{\beta}{\Delta}\{D\theta_{24}+\varphi_{13}^{\eta}(\theta_{13}s-\theta_{24}\varkappa_{13})+\varphi_{1-4}^{\eta}(-\theta_{24}s+\theta_{13}\varkappa_{24})\},
\end{aligned} \tag{3.6}$$

$$e_{32}=-e_{31}, \tag{3.7}$$

where

$$\Delta = D^2 - D(\varphi^{\eta}_{13}\varkappa_{13} + \varphi^{\eta}_{24}\varkappa_{24} + 2\varphi^{\eta}_{1-4}s) + \Big[\varphi^{\eta}_{13}\varphi^{\eta}_{24} - (\varphi^{\eta}_{1-4})^2\Big](\varkappa_{13}\varkappa_{24} - s^2). \quad (3.8)$$

Similarly, using the single-particle distribution functions (2.10) and the relations (2.16), we find the static dielectric susceptibility of a clamped KD_2PO_4 crystal along the c-axis

$$\chi^{\varepsilon}_{33}(0,T,\sigma_{12}) = \left(\frac{\partial P_3}{\partial E_3}\right)_{\varepsilon_{12}} = \chi^0_{33} + \frac{\mu_{13}}{\bar{v}}\left(\frac{\partial \eta^{(1)z}_{13}}{\partial E_3}\right)_{\varepsilon_{12}} + \frac{\mu_{24}}{\bar{v}}\left(\frac{\partial \eta^{(1)z}_{24}}{\partial E_3}\right)_{\varepsilon_{12}}. \quad (3.9)$$

The quantities $\left(\frac{\partial \eta^{(1)z}_{13}}{\partial E_3}\right)_{\varepsilon_{12}}$ and $\left(\frac{\partial \eta^{(1)z}_{24}}{\partial E_3}\right)_{\varepsilon_{12}}$ obey the following system of equations

$$\begin{aligned} N_{11}\left(\frac{\partial \eta^{(1)z}_{13}}{\partial E_3}\right)_{\varepsilon_{12}} + N_{12}\left(\frac{\partial \eta^{(1)z}_{24}}{\partial E_3}\right)_{\varepsilon_{12}} &= N^E_1, \\ N_{21}\left(\frac{\partial \eta^{(1)z}_{13}}{\partial E_3}\right)_{\varepsilon_{12}} + N_{22}\left(\frac{\partial \eta^{(1)z}_{24}}{\partial E_3}\right)_{\varepsilon_{12}} &= N^E_2, \end{aligned} \quad (3.10)$$

where

$$N^E_1 = \frac{\beta\mu_{13}}{2}\varkappa_{13} + \frac{\beta\mu_{24}}{2}s; \quad N^E_2 = \frac{\beta\mu_{13}}{2}s + \frac{\beta\mu_{24}}{2}\varkappa_{24}. \quad (3.11)$$

It yields

$$\begin{aligned} &\chi^{\varepsilon}_{33}(0,T,\sigma_{12}) = \chi^{0\varepsilon}_{33} + \bar{v}\frac{\mu^2_{13}}{v^2}\frac{1}{2T\Delta}[D\varkappa_{13} - \varphi^{\eta}_{24}(\varkappa_{13}\varkappa_{24} - s^2)] \\ &+\bar{v}\frac{\mu^2_{24}}{v^2}\frac{1}{2T\Delta}[D\varkappa_{24} - \varphi^{\eta}_{13}(\varkappa_{13}\varkappa_{24} - s^2)]\bar{v}\frac{\mu_{13}\mu_{24}}{v^2}\frac{1}{T\Delta}[Ds - \varphi^{\eta}_{1-4}(\varkappa_{13}\varkappa_{24} - s^2)]. \end{aligned} \quad (3.12)$$

Constants of the piezoelectric stress

$$h_{31} = -\left(\frac{\partial E_1}{\partial \varepsilon_1}\right)_{P_3}, \quad h_{32} = -\left(\frac{\partial E_1}{\partial \varepsilon_2}\right)_{P_3}, \quad (3.13)$$

using the system of equations

$$\begin{aligned} N_{11}\left(\frac{\partial \eta^{(1)z}_{13}}{\partial \varepsilon_1}\right)_{P_3} + N_{12}\left(\frac{\partial \eta^{(1)z}_{24}}{\partial \varepsilon_1}\right)_{P_3} &= N^{\varepsilon}_1 + N^E_1\left(\frac{\partial E_3}{\partial \varepsilon_1}\right)_{P_3}, \\ N_{21}\left(\frac{\partial \eta^{(1)z}_{13}}{\partial \varepsilon_1}\right)_{P_3} + N_{22}\left(\frac{\partial \eta^{(1)z}_{24}}{\partial \varepsilon_1}\right)_{P_3} &= N^{\varepsilon}_2 + N^E_2\left(\frac{\partial E_3}{\partial \varepsilon_1}\right)_{P_3}, \end{aligned} \quad (3.14)$$

and the expression (2.17), are found in the following form

$$h_{31} = \frac{e_{31}}{\chi^{\varepsilon}_{33}}, \qquad h_{32} = \frac{e_{32}}{\chi^{\varepsilon}_{33}}. \quad (3.15)$$

Let us now calculate the elastic characteristics of a KD_2PO_4 crystal under the stress σ_{12}. From (2.16) and solutions of (3.2) we obtain the elastic constants at a constant field

$$
\begin{aligned}
c_{11}^{E} &= \left(\frac{\partial\sigma_1}{\partial\varepsilon_1}\right)_{E_3} = \left\{c_{11}^{0E} - \frac{2\psi_{12}}{\bar{v}}\left(\eta_{13}^{(1)}e_{13} - \eta_{24}^{(1)}e_{24}\right) - \frac{2\delta_{12}\psi_{12}}{\bar{v}D_{12}T}\left(\eta_{13}^{(1)}t_{13} - \eta_{24}^{(1)}t_{24}\right)\right.\\
&\quad - \frac{2\delta_{12}}{\bar{v}D_{12}}[(\varphi_{13}^{\eta}t_{13} + \varphi_{1-4}^{\eta}t_{24})e_{13} + (\varphi_{1-4}^{\eta}t_{13} + \varphi_{24}^{\eta}t_{24})e_{24}]\\
&\quad + \frac{2\delta_{12}^2}{\bar{v}D_{12}^2T}\left(2bc_{12}\cosh z_{13} - 2\frac{b}{c_{12}}\cosh z_{24}\right)^2\\
&\quad \left. - \frac{2\delta_{12}^2}{\bar{v}D_{12}T}\left(2bc_{12}\cosh z_{13} + 2\frac{b}{c_{12}}\cosh z_{24}\right)\right\}\\
&\quad = c_{11}^{0E} - c^{E}(12),\\
c_{12}^{E} &= \left(\frac{\partial\sigma_1}{\partial\varepsilon_2}\right)_{E_3} = \left(\frac{\partial\sigma_2}{\partial\varepsilon_1}\right)_{E_3} = c_{12}^{0E} + c^{E}(12),\\
c_{22}^{E} &= \left(\frac{\partial\sigma_2}{\partial\varepsilon_2}\right)_{E_3} = c_{22}^{0E} - c^{E}(12).
\end{aligned}
\tag{3.16}
$$

From (2.16) and solutions of the systems (3.2) and (3.6), we find the elastic constants at constant polarization

$$
c_{11}^{P} = c_{11}^{E} + e_{31}h_{31}, \tag{3.17}
$$

$$
\begin{aligned}
c_{12}^{P} &= c_{12}^{E} + e_{32}h_{31} = c_{12}^{E} - (e_{32}h_{32})\cdot 10^{-2},\\
c_{22}^{P} &= c_{22}^{E} + e_{32}h_{32}.
\end{aligned}
\tag{3.18}
$$

Elastic compliances $\left(\frac{\partial\varepsilon_1}{\partial\sigma_1}\right)_{E_3} = s_{11}^{E}$, $\left(\frac{\partial\varepsilon_2}{\partial\sigma_1}\right)_{E_3} = s_{21}^{E}$ obey the system of equations

$$
\begin{aligned}
&c_{11}^{E}s_{11}^{E} + c_{12}^{E}s_{12}^{E} = 1, \qquad c_{12}^{E}s_{22}^{E} + c_{11}^{E}s_{12}^{E} = 0,\\
&c_{12}^{E}s_{11}^{E} + c_{22}^{E}s_{12}^{E} = 0, \qquad c_{22}^{E}s_{22}^{E} + c_{12}^{E}s_{12}^{E} = 1.
\end{aligned}
\tag{3.19}
$$

Hence

$$
s_{11}^{E} = \frac{c_{22}^{E}}{c_{11}^{E}c_{22}^{E} - (c_{12}^{E})^2}, \quad s_{12}^{E} = \frac{c_{12}^{E}}{c_{11}^{E}c_{22}^{E} - (c_{12}^{E})^2}, \quad s_{22}^{E} = \frac{c_{11}^{E}}{c_{11}^{E}c_{22}^{E} - (c_{12}^{E})^2}. \tag{3.20}
$$

From (3.20) we obtain expressions for the constants of piezoelectric strain and for compliances at constant polarization

$$
g_{31} = h_{31}(s_{11}^{P} - s_{12}^{P}), \quad g_{32} = h_{31}(s_{12}^{P} - s_{22}^{P}), \tag{3.21}
$$

$$
s_{11}^{P} = \frac{c_{22}^{P}}{c_{11}^{P}c_{22}^{P} - (c_{12}^{P})^2}, \quad s_{12}^{P} = \frac{c_{12}^{P}}{c_{11}^{P}c_{22}^{P} - (c_{12}^{P})^2}, \quad s_{22}^{P} = \frac{c_{11}^{P}}{c_{11}^{P}c_{22}^{P} - (c_{12}^{P})^2}. \tag{3.22}
$$

The coefficient of piezoelectric strain

$$
d_{31} = \left(\frac{\partial P_3}{\partial\sigma_1}\right)_{E_3} = \frac{\mu_{13}}{v}\left(\frac{\partial\eta_{13}^{(1)}}{\partial\sigma_1}\right)_{E_3} + \frac{\mu_{24}}{v}\left(\frac{\partial\eta_{24}^{(1)}}{\partial\sigma_1}\right)_{E_3}. \tag{3.23}
$$

can be found from the system of equations

$$N_{11}\left(\frac{\partial\eta_{13}^{(1)}}{\partial\sigma_1}\right)_{E_3} + N_{12}\left(\frac{\partial\eta_{24}^{(1)}}{\partial\sigma_1}\right)_{E_3} = N_1^{\varepsilon}\left(\frac{\partial\varepsilon_1}{\partial\sigma_1}\right)_{E_3} - N_2^{\varepsilon}\left(\frac{\partial\varepsilon_2}{\partial\sigma_1}\right)_{E_3},$$
$$N_{21}\left(\frac{\partial\eta_{13}^{(1)}}{\partial\sigma_1}\right)_{E_3} + N_{22}\left(\frac{\partial\eta_{24}^{(1)}}{\partial\sigma_1}\right)_{E_3} = N_2^{\varepsilon}\left(\frac{\partial\varepsilon_1}{\partial\sigma_1}\right)_{E_3} - N_2^{\varepsilon}\left(\frac{\partial\varepsilon_2}{\partial\sigma_1}\right)_{E_3}$$

in the following form

$$d_{31} = e_{31}s_{11}^E + e_{32}s_{21}^E = e_{31}(s_{11}^E - s_{12}^E). \tag{3.24}$$

Similarly

$$d_{32} = e_{31}s_{12}^E + e_{32}s_{22}^E = e_{31}(s_{12}^E - s_{22}^E).$$

Since

$$d_{31} = \left(\frac{\partial\varepsilon_1}{\partial E_3}\right)_{\sigma} \quad \text{and} \quad d_{32} = \left(\frac{\partial\varepsilon_2}{\partial E_3}\right)_{\sigma},$$

we can also find the longitudinal dielectric susceptibility of a free crystal (σ = const)

$$\chi_{33}^{\sigma}(0,T,\sigma_{12}) = \chi_{33}^{\varepsilon} + e_{31}(d_{31} - d_{32}). \tag{3.25}$$

Since the stress σ_{12} lowers down the crystal symmetry, the static dielectric susceptibilities along the a and b axes are different. The transverse susceptibility along the a-axis is

$$\chi_{11}(0,T,\sigma_{12}) = \chi_{11}^0 + \bar{v}\frac{\mu_1^2}{v^2}\frac{1}{T}\frac{2(a + b/c_{12}\cosh z_{24})}{D_{12}^a}, \tag{3.26}$$

where

$$D_{12}^a = D_{12} - 2(a + b/c_{12}\cosh z_{24})[1/(1-\eta_{13}^{(1)2}) + \beta(\nu_1 - \nu_3) + (\psi_1 - \psi_3)\varepsilon_{12})],$$

whereas that along the b-axis is

$$\chi_{22}(0,T,\sigma_{12}) = \chi_{11}^0 + \bar{v}\frac{\mu_2^2}{v^2}\frac{1}{T}\frac{2(a + bc_{12}\cosh z_{13})}{D_{12}^b}, \tag{3.27}$$
$$D_{12}^b = D_{12} - 2(a + bc_{12}\cosh z_{13})[1/(1-\eta_{24}^{(1)2}) + \beta(\nu_1-\nu_3) - (\psi_1-\psi_3)\varepsilon_{12})].$$

4. Discussion

For numerical estimate of mechanical stress σ_{12} and temperature dependences of the characteristics calculated in the previous section, we use the values of the theory parameters, obtained in [6,7]. These values provide a good description of experimental data for thermodynamic and dynamic characteristics of KD_2PO_4: ε = 93 K, w = 840 K, $w_1 = \infty$, ν =37.44 K, $\bar{\nu}$ =16 K at T_c = 219.7 K.

The strain ε_{12} splits the energies of one and three-particle deuteron configurations w. The splitting is attributed mostly to the changes in the D-site distances:

$\Delta w/w \sim 2\Delta\delta/\delta$. Under hydrostatic pressure $\Delta\delta/\delta \sim -1\%/\text{kbar}$ [8], and the changes of O-O and D-D distances are accompanied by rotation of PO_4 tetrahedra. Since the symmetrized stress σ_{12} presumably does not lead to the tetrahedra rotation, the changes in the D-site distances here are assumed to be approximately twice as large as those in the hydrostatic pressure case at the same value of external stress. Therefore, at σ_{12} stress $\Delta\delta/\delta \sim \pm 2\%/\text{kbar}$, and $\delta_w = \Delta w/w = \delta_{12}\varepsilon_{12}/w \sim 4\ \%/\text{kbar}$.

In this paper we obtained a microscopic expression for a deuteron subsystem contribution $c(12)$ to the elastic constants. The contributions of other mechanisms to c_{11} and c_{12} are taken into account implicitly by a proper choice of the "seed" temperature independent elastic constants $c_{11}^{(0)}$ and $c_{12}^{(0)}$. Calculations have shown that the parameter ψ_{12} hardly affects the physical characteristics of a crystal; we set $\psi_{12} = 600$ K. Hence, the values of the elastic constants c_{11} and c_{12} in the paraelectric phase at zero stress $\sigma_{12} = 0$ are determined by the deformation potential δ_{12} and the "seed" elastic constants $c_{11}^{(0)}$ and $c_{12}^{(0)}$.

Figure 1 illustrates how the presented theory describes the experimental temperature dependence of the elastic constants c_{11} and c_{12} at $\sigma_{12} = 0$ and different values of δ_{12}.

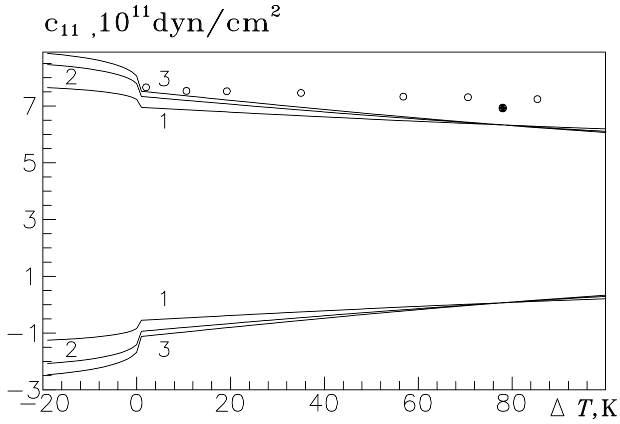

Figure 1. Dependences of the elastic constants c_{11} and c_{12} on temperature at different values of δ_{12} : 1 – 18440; 2 – 23500; 3 – 25580. Experimental points are taken from [9,10].

As will be shown below, the contribution of a deuteron subsystem $c(12)$ to the elastic constants is negative and increases with temperature and with δ_{12} (see figure 1). The deformation potential δ_{12} also increases the slope $|\partial c_{11}/\partial T|$. According to [9], the elastic constant c_{12} of KH_2PO_4 hardly depends on temperature. Within our approach, $c_{11} = c_{11}^{(0)} - c(12)$, and $c_{12} = c_{12}^{(0)} + c(12)$. Therefore, if c_{11} is a decreasing function of temperature, then c_{12} is an increasing one.

It is experimentally found [9] that the relative change in the elastic constant c_{11} $\delta_c = c_{11}(T_c + 80\text{ K})/c_{11}(T_c) - 1$ for KH_2PO_4 crystals is about $\sim 9\%$. For deuterated crystals $K(H_{0.11}D_{0.89})_2PO_4$ at $T = T_c + 72$ K $c_{11} = 6.93 \cdot 10^{11}$ dyn/cm^2 and $c_{12} = -0.71 \cdot 10^{11}$ dyn/cm^2 [10]. For completely deuterated KD_2PO_4 at $T = T_c + 72$ K we take $c_{11} \approx 6.4 \cdot 10^{11}$ dyn/cm^2, extrapolating the values of the elastic constants of KH_2PO_4 and $K(H_{0.11}D_{0.89})_2PO_4$ at this temperature.

However, the calculations show that at no set of the parameters δ_{12} and $c_{11}^{(0)} - c_{12}^{(0)}$ it is possible to simultaneously obtain the correct values of $\delta_w = 4\%$/kbar, as well as correct value and temperature variation of the elastic constant $c_{11} = 6.4 \cdot 10^{11}$ dyn/cm^2 and $\delta_c \sim 9$ %. The value of δ_w increases with δ_{12}, but it is still smaller than 4%/kbar even at $\delta_{12} = 25935$ K, where the ferroelectric phase vanishes, and $\delta_c \sim 20\%$. At $\delta_{12} = 18440$ K and $c_{11}^0 = 7.76 \cdot 10^{11}$ dyn/cm^2 we have $\delta_c = 9\%$, but then $\delta_w = 2\%$/kbar, and the phase transition in stress disappears.

Hence we use such values of the deformation potential δ_{12} and "seed" elastic constants that provide a good fit both to the ratio δ_w and to the temperature curve of the elastic constant c_{11}: $\delta_{12} = 23500$ K, $c_{11}^{(0)} = 8.65 \cdot 10^{11}$ K, $c_{11}^{(0)} = -2.25 \cdot 10^{11}$ K. At these values we obtain $\delta_w = 3.4$ %/kbar, and $\delta_c = 12.8\%$.

The strain ε_{12} also affects the effective dipole moments μ_i of hydrogen bonds. It is usually assumed that these dipole moments are proportional to the distance δ between the equilibrium deuteron sites on a bond. Since the value of δ at bonds going along the axis a is increased, whereas that at bonds going along the axis b is decreased, then

$$
\begin{aligned}
&\mu_{13} = \mu_{23} = \mu_{33} = \mu_3[1 - \frac{\delta_1}{\delta_0}\frac{1}{2}(c_{11}^{(0)} - c_{12}^{(0)})\varepsilon_{12}],\\
&\mu_{24} = \mu_{23} = \mu_{43} = \mu_3[1 + \frac{\delta_1}{\delta_0}\frac{1}{2}(c_{11}^{(0)} - c_{12}^{(0)})\varepsilon_{12}],\\
&\mu_1 \cos\gamma = \mu_{11} = -\mu_{31} = \mu_\perp \cos\gamma[1 - \frac{\delta_1}{\delta_0}\frac{1}{2}(c_{11}^{(0)} - c_{12}^{(0)})\varepsilon_{12}],\\
&\mu_1 \sin\gamma = -\mu_{21} = \mu_{41} = \mu_\perp \sin\gamma[1 + \frac{\delta_1}{\delta_0}\frac{1}{2}(c_{11}^{(0)} - c_{12}^{(0)})\varepsilon_{12}],\\
&\mu_2 \cos\gamma = -\mu_{22} = \mu_{42} = \mu_\perp \cos\gamma[1 + \frac{\delta_1}{\delta_0}\frac{1}{2}(c_{11}^{(0)} - c_{12}^{(0)})\varepsilon_{12}],\\
&\mu_2 \sin\gamma = \mu_{12} = -\mu_{32} = \mu_\perp \sin\gamma[1 - \frac{\delta_1}{\delta_0}\frac{1}{2}(c_{11}^{(0)} - c_{12}^{(0)})\varepsilon_{12}],
\end{aligned}
$$

where $\delta_1/\delta_0 = -0.02 \cdot 10^{-3}$ at $\sigma_{12} > \sigma_{12}(0K)$ $\delta_1/\delta_0 = -0.02 \cdot 10^{-4}$ bar^{-1}, $\mu_3(T < T_c) = 1.8 \cdot 10^{-18}$ esu cm, $\mu_3(T > T_c) = 2.66 \cdot 10^{-18}$ esu cm, $\mu_\perp = 2.8 \cdot 10^{-18}$ esu cm.

In figure 2 we show the phase diagrams calculated at different values of the parameter δ_{12}. As has already been shown [3,4], the σ_{12} stress can induce a a new phase, of presumably monoclinic symmetry with the strain ε_{12} significantly larger than at stresses right below the critical one.

The phase diagrams obtained in our calculations consist of the three phases: I – the regular paraelectric phase with ε_{12}^I and $\eta_{13}^{(1)} = \eta_{24}^{(1)} = 0$, II – the ferroelectric phase where $\eta_{13}^{(1)} \neq 0, \eta_{24}^{(1)} \neq 0$; III – a new paraelectric phase where ($\eta_{13}^{(1)} = \eta_{24}^{(1)} = 0$, but $\varepsilon_{12}^{III} \gg \varepsilon_{12}^I$ (dependences of strain on stress are discussed below). The curve AO, separating regions I and II, corresponds to the ferroelectric first order phase transition in $\eta_{13}^{(1)}$ and $\eta_{24}^{(1)}$ parameters, $T_c(A) = 219.7$ K; temperature of the ferroelectric

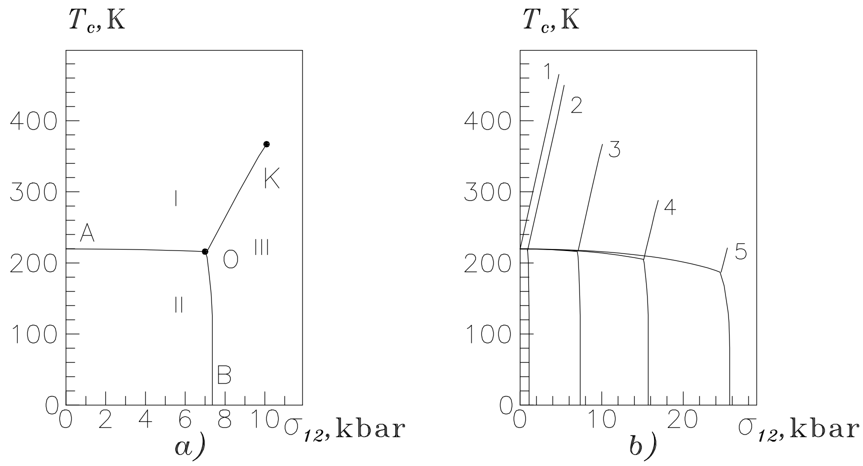

Figure 2. The phase diagram of a KD_2PO_4 crystal at different values of δ_{12} (K) (a) – 23500; (b): 1 – 25935; 2 – 25580; 3 – 23500; 4 – 21000; 5 – 18440.

transition decreases with stress. The lines OK and OB denote the first order phase transitions to the monoclinic phase III. At stresses above $\sigma_{12}(B)$ ($\sigma_{12}(B) = 7.36$ kbar at δ_{12}=23500 K) the ferroelectric phase disappears. Coordinates of the tricritical point O are $T_\mathrm{c}(O) = 215.9$ K, $\sigma_{12}(O) = 7.11$ kbar (at δ_{12}=23500 K).

On increasing stress along the line OK of the first order transitions from tetragonal to monoclinic phase, jumps of strain at the transition decrease (see below). This line terminates at the critical point K ($T_\mathrm{c}(K) = 370$ K, $\sigma_{12}(K) = 10.1$ kbar at δ_{12}=23500 K), where the jump of strain turns to zero.

Major effects of the increase in δ_{12} are the shift of the phase III to the smaller stresses, increase in the value of $T_\mathrm{c}(K)$ and decrease in $\sigma_{12}(K)$. At $\delta_{12} = 25935$ K the ferroelectric phase disappears from the phase diagram. Dependence of the ferroelectric phase transition temperature also slightly changes with the value of δ_{12}.

The above results partially accord with those obtained by Stasyuk and Biletskii [4]. However, in our calculations the monoclinic phase is purely paraelectric ($\eta_{13}^{(1)} = \eta_{24}^{(1)} = 0$), whereas in [4] the order parameters in this phase are different from zero. Stasyuk and Biletskii also predict high-stress second order phase transitions in $\eta_{13}^{(1)}$ and $\eta_{24}^{(1)}$ between monoclinic and tetragonal phases. In our calculations those transitions, naturally, do not emerge ($\eta_{13}^{(1)} = \eta_{24}^{(1)} = 0$ in both phases).

Let us now consider the stress σ_{12} effects on the above calculated physical characteristics of the crystals. As follows from the phase diagram, temperature and stress behaviour of the characteristics depend on the number of the phase transitions being undergone by the system. We can separate several types of behaviour; some of them will be illustrated in figures below.

Thus, there are four kinds of temperature behaviour:

- $\sigma_{12} < \sigma_{12}(O)$ (curves $1' - 4'$ in figures 6–16). On changing temperature the system undergoes a single first order phase transition between the paraelectric and ferroelectric phases I and II, with the transition temperature being lowered by the stress along the line AO of the phase diagram. Temperature curves of the physical characteristics are similar to those at atmospheric pressure but shifted to lower temperatures.

- $\sigma_{12}(O) < \sigma_{12} < \sigma_{12}(B)$ (curves $5'$ in figures 6–16). On changing temperature the system undergoes two first order phase transitions – between paraelectric tetragonal and monoclinic phases I and III and between the monoclinic and ferroelectric phases III and II. Temperature curves of the physical characteristics have two peculiarities at both transitions. In figures, however, only the upper transition between the phases III and II is seen.

- $\sigma_{12}(B) < \sigma_{12} < \sigma_{12}(K)$ (curves $6'$ - $7'$ in figures 6–16). On changing temperature the system undergoes the first order phase transition between paraelectric tetragonal and monoclinic phases I and III. Temperature curves of the physical characteristics have a single peculiarity at the transition point and shift to higher temperatures with increasing σ_{12}.

- $\sigma_{12} > \sigma_{12}(K)$ (curves $8'$ in figures 6–16). There are no phase transitions. Temperature behaviour of the physical characteristics is smooth and specific to the monoclinic phase.

We can also name four types of stress behaviour:

- $T < T_{\mathrm{c}}(O)$ (curves 1 in figures 6–16). On changing stress the system undergoes a single first order phase transition between the ferroelectric and monoclinic phases II and III, with the transition stress decreasing with temperature (along the line OB of the phase diagram). Stress curves of the physical characteristics have a peculiarity at the phase transition.

- $T_{\mathrm{c}}(O) < T < T_{\mathrm{c}}(A)$ (curves 2 in figures 6–16). On changing stress the system undergoes two first order phase transitions – between ferroelectric and paraelectric tetragonal phase II and I and between the tetragonal and monoclinic phases I and III. Stress curves of the physical characteristics have two peculiarities at both transitions.

- $T_{\mathrm{c}}(A) < T < T_{\mathrm{c}}(K)$ (curves 3 – 5 in figures 6–16). On changing stress the system undergoes the first order phase transition between paraelectric tetragonal and monoclinic phases I and III. Stress curves of the physical characteristics have a single peculiarity at the transition point and shift to higher stresses with increasing temperature. Magnitude of the peculiarity decreases with temperature and vanishes at the critical point K.

- $T > T(K)$ (curves 6 in figures 6–16). There are no phase transitions. Stress behaviour of the physical characteristics is smooth and specific to the monoclinic phase.

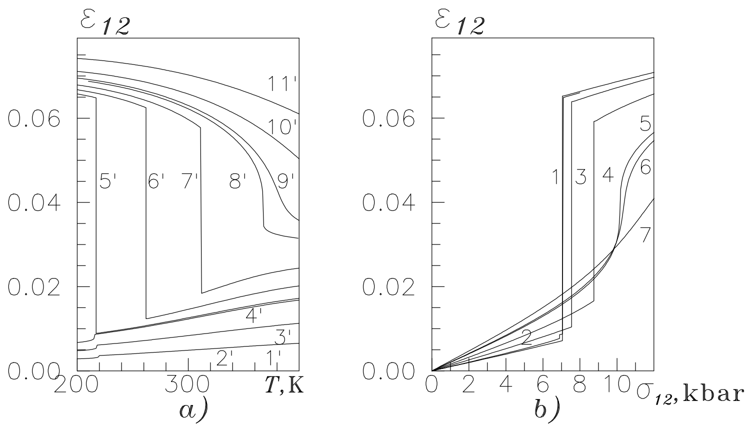

Figure 3. Dependences of strain ε_{12} on temperature at different values of stress σ_{12} (kbar) (a): 1' – 0; 2' – 3; 3' – 5; 4' – 7; 5' – 7.36; 6' – 8; 7' – 9; 8' – 10.09; 9' – 10.5; 10' – 12; 11' – 15 and on stress σ_{12} at different values of temperature T(K) (b): 1 – 210; 2 – 218; 3 – 240; 4 – 300; 5 –370 ; 6 – 380; 7 – 450.

The above presented types of temperature and stress dependences of the physical characteristics are well illustrated by the plotted in figure 3 curves of strain ε_{12}.

Curves $1' - 4'$ here exhibit the first type of temperature behaviour with a single jump of strain at the ferroelectric phase transition; the strain ε_{12} increases with temperature in both tetragonal and ferroelectric phases. Curves $5' - 8'$ are characteristic to the third type of temperature behaviour – a huge downward jump of ε_{12} at the transition from monoclinic to the tetragonal phase. Magnitude of the jumps decreases with the stress and vanishes at the critical point K. Above the jumps the strain ε_{12} has a typical paraelectric increasing behaviour. Curves $9' - 11'$ have no peculiarities and reveal a decreasing temperature behaviour of ε_{12} in the monoclinic phase.

Very specific to the stress curves of strain $\sigma_{12}(\varepsilon_{12})$ is the possibility to have two extrema and the bending point. Coordinates of the bending point can be found from the condition $g_{1E}(12, \varepsilon_{12}^{I,II}) = g_{1E}(12, \varepsilon_{12}^{III})$. At this point there occurs a first order phase transition to a new phase with a strain ε_{12} being much higher than right below the transition. The transition stress depends of the values of the parameters w, δ_{12}, c_{11}^0, c_{12}^0 and on temperature. Both a decrease in w, c_{11}^0, and c_{12}^0 and an increase in δ_{12} lower it down. Two extrema and the bending point (the transition to the new phase III) are possible only if

$$\frac{\delta_{12}^2}{c_{11}^0 - c_{12}^0} > \frac{2\bar{v}T[(1+2a+d)^2 - 4b^2]}{(1+2a+d)^2}.$$

As one can see in figure 3b, the stress σ_{12} increases the strain ε_{12} in all phases. Curve 1 is specific to the first type of stress behaviour with a single jump at the transition to the monoclinic phase. Rate of the changes in ε_{12} with the stress σ_{12} are nearly the same in both ferroelectric and monoclinic phases. Instead, curve 2 has two jumps (second type of stress behaviour) – at the ferroelectric-paraelectric

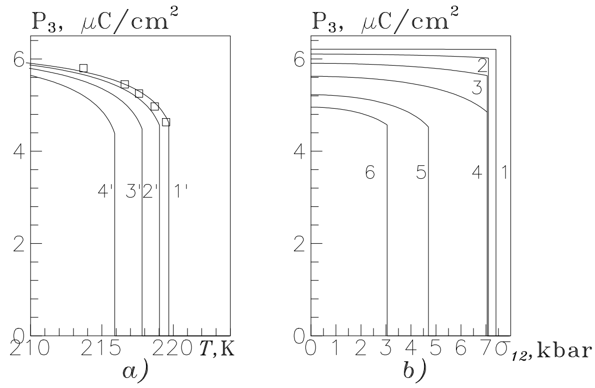

Figure 4. Dependences of polarization P_3 on temperature at different values of stress σ_{12} (kbar) (a): 1' – 0; 2' – 3; 3' – 5; 4' – 7 and on stress σ_{12} at different temperatures T(K) (b): 1 – 150; 2 – 200; 3 – 210; 4 – 215; 5 – 218; 6 – 219. Experimental points are taken from [11].

and paraelectric tetragonal-monoclinic phase transitions, jump at the ferroelectric transition being much smaller. Curves 3 – 5 exhibit a single jump of the strain at the transition to the monoclinic phase; the jump magnitude decreases with temperature and vanishes at the critical point. At higher temperature (curves 6 and 7) the strain has a smooth stress behaviour.

In figure 4 we depict the stress and temperature dependences of polarization P_3. Since polarization exists only in the ferroelectric phase, only the first type of stress or temperature behaviour is possible. Therefore, temperature curves of polarization are not changed by stress but shifted to lower temperatures due to lowering the ferroelectric phase transition temperature. When temperatures are low (polarization is saturated), P_3 is hardly affected by the stress σ_{12} except for a jump to zero at the transition to the monoclinic paraelectric phase. At temperatures close to $T_{\mathrm{c}}(A)$ (transition temperature at ambient pressure), the stress reduces the magnitude of polarization and its jump at the transition point.

Let us now consider the temperature and stress curves of the elastic characteristics. Temperature dependence of the contribution of the deuteron subsystem to the elastic constants $c(12)$ at low stresses in the vicinity of the ferroelectric phase transition is shown in figure 5. As one can see, an increase in stress raises up the value of $c(12)$ in the paraelectric phase and enhances its variation with temperature.

Temperature and stress curves of all calculated elastic constants are shown in figures 6–9.

The constants c^P and c^E coincide in the paraelectric phase. Their behaviour with temperature and stress is well described by the above formulated rules. At low stresses, c_{11}^P and c_{11}^E have downward jumps at the transition from the ferroelectric to the paraelectric tetragonal phase, whereas c_{12}^P and c_{12}^E have upward jumps. With increasing stress, the jumps transform to peaks with increasing magnitudes. At the transition to the monoclinic phase, only small jumps in the elastic constants are observed.

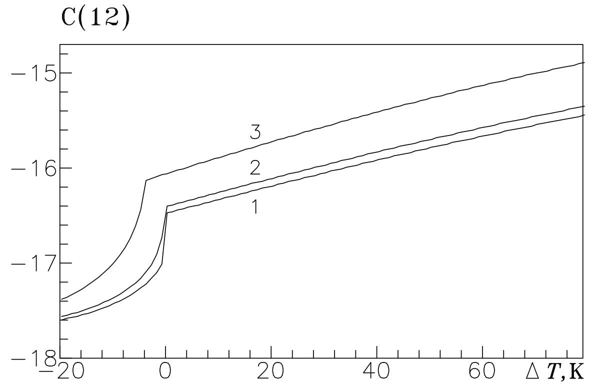

Figure 5. Temperature dependence of the deuteron subsystem contribution to the elastic constants c_{11} and c_{12} at different stresses σ_{12} (kbar) : 1 – 0; 2 – 3; 3 – 5.

Character of temperature and stress behaviour of the elastic compliances is opposite to that of the elastic constants: where c_{11} and c_{12} decrease and have a minimum, the compliances s_{11} and s_{12} increase and have a maximum.

In figures 10 and 11 we plot the stress and temperature dependences of the coefficients of piezoelectric stress e_{31} and piezoelectric strain d_{31}. The coefficients are negative and differ from zero only in the ferroelectric phase II. At temperatures lower than 175 K e_{31} and d_{31} are also practically equal to zero. On approaching the transition point, e_{31} and d_{31} decrease with temperature (or stress), having a sharp negative peak at the paraelectric-ferroelectric phase transition and jumping upward to zero just above the transition point. The magnitude of the peaks in the temperature dependences of e_{31} and d_{31} increases with the stress.

Shown in figures 12 and 13 temperature and stress dependences of the constants of piezoelectric stress h_{31} and of piezoelectric strain g_{31} are qualitatively similar to those of e_{31} and d_{31}. The difference is, h_{31} and g_{31} are increasing functions of temperature in the ferroelectric phase and have jumps instead of peaks at the transition to a paraelectric phase.

The stress and temperature dependences of the clamped static dielectric permittivity $\varepsilon_3^{\varepsilon}(0, T, \sigma_{12})$ are depicted in figure 14.

Below the critical stress $\sigma_{12}(O)$ (curves 1' – 4' in figure 14a) the permittivity exhibits a regular Curie-Weiss behaviour in the paraelectric phase and has a peak at the transition point, with the peak magnitude increasing with σ_{12}. At higher stresses $\sigma_{12}(O) < \sigma_{12} < \sigma_{12}^K$ (curves 5' and 6') the permittivity has a downward jump at the transition to the monoclinic phase III and remains temperature independent in the phase III. At $\sigma_{12} > \sigma_{12}^K$ where there exists only a monoclinic phase, the permittivity hardly depends on temperature.

Stress behaviour of the longitudinal permittivity is very well described by the formulated rules. Two peculiarities of $\varepsilon_3^{\varepsilon}(0, T, \sigma_{12})$ are seen in curve 2 (two phase transitions between the phases II and I and between I and III).

Let us consider now the stress and temperature dependences of transverse static

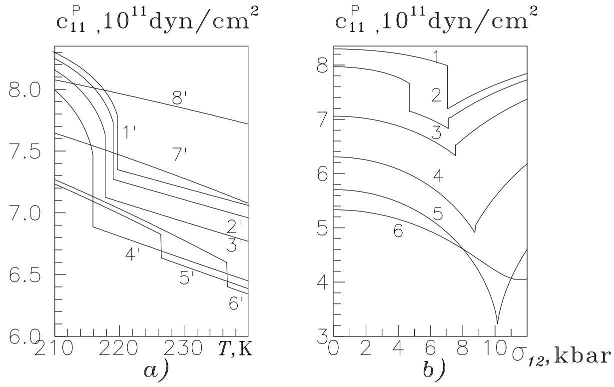

Figure 6. Dependences of the elastic constants c_{11}^P on temperature at different values of stress σ_{12} (kbar) (a): 1' – 0; 2' – 3; 3' – 5; 4' – 7; 5' – 7.3; 6' – 7.5; 7' – 10; 8' – 15; and on σ_{12} at different values of temperature T(K) (b): 1 – 210; 2 – 218; 3 – 240; 4 – 300; 5 – 370; 6 – 450.

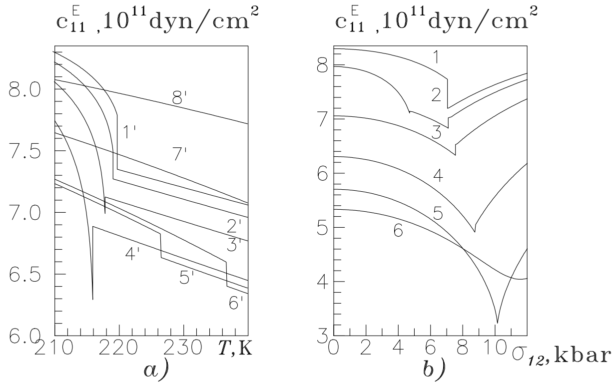

Figure 7. Dependences of the elastic constants c_{11}^E on temperature at different stresses σ_{12} (a) and on σ_{12} (b) at different temperatures. Values of stress and temperature are the same as in figure 6.

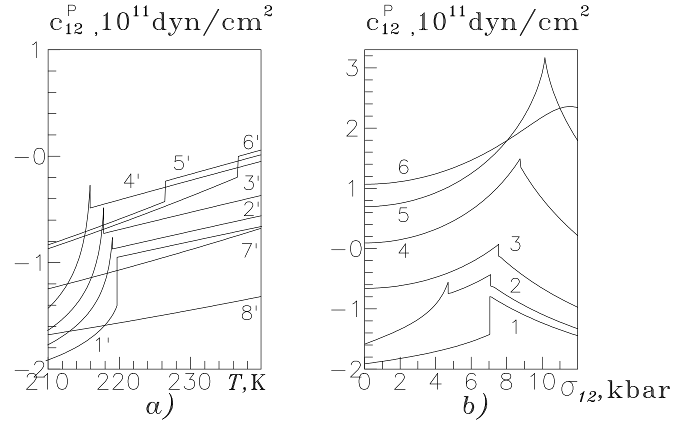

Figure 8. Dependences of the elastic constants c_{12}^{P} on temperature at different stresses σ_{12} (a) and on σ_{12} (b) at different temperatures. Values of stress and temperature are the same as in figure 6.

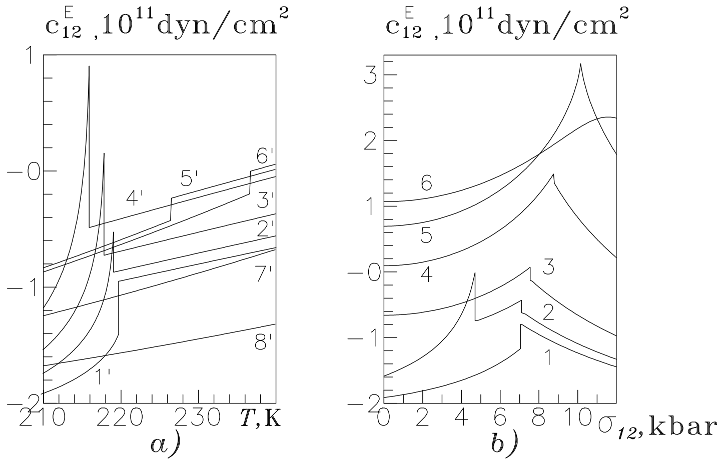

Figure 9. Dependences of the elastic constants c_{12}^{E} on temperature at different stresses σ_{12} (a) and on σ_{12} (b) at different temperatures. Values of stress and temperature are the same as in figure 6.

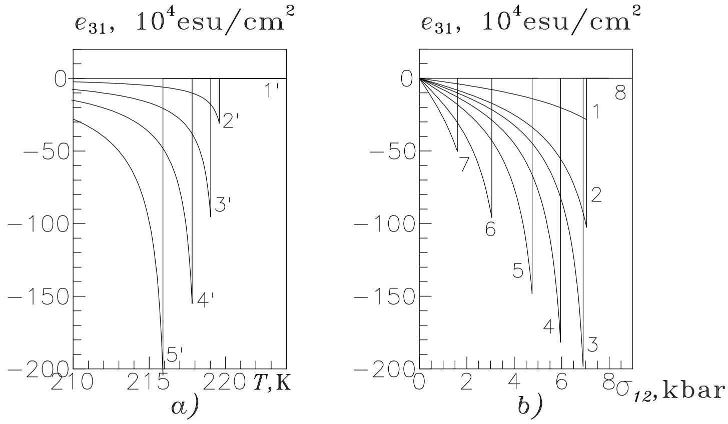

Figure 10. Dependences of the coefficient of piezoelectric stress e_{31} on temperature at different stresses σ_{12} (a) and on σ_{12} (b) at different temperatures. Values of stress and temperature are the same as in figure 6.

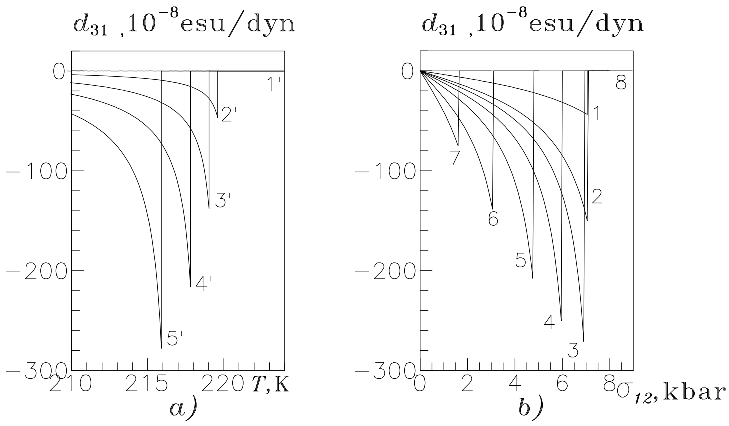

Figure 11. Dependences of the coefficient of piezoelectric strain d_{31} on temperature at different stresses σ_{12} (a) and on σ_{12} (b) at different temperatures. Values of stress and temperature are the same as in figure 6.

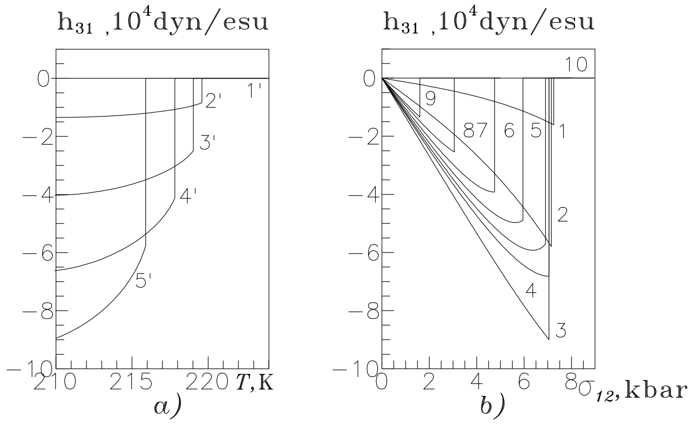

Figure 12. Dependences of the constant of piezoelectric stress h_{31} on temperature at different stresses σ_{12} (a) and on σ_{12} (b) at different temperatures. Values of stress and temperature are the same as in figure 6.

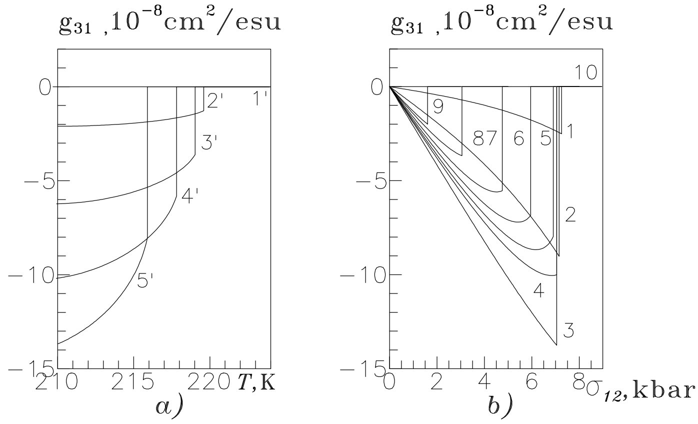

Figure 13. Dependences of the constant of piezoelectric strain g_{31} on temperature at different stresses σ_{12} (a) and on σ_{12} (b) at different temperatures. Values of stress and temperature are the same as in figure 6.

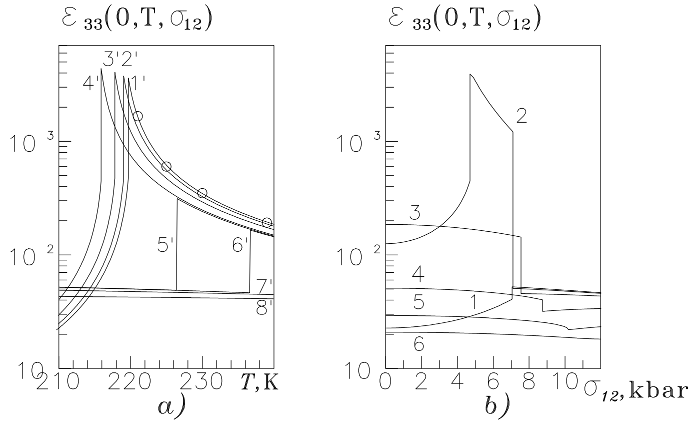

Figure 14. Dependences of clamped static dielectric permittivity $\varepsilon_{33}^{\varepsilon}$ on temperature at different stresses σ_{12} (a) and on σ_{12} (b) at different temperatures. Values of stress and temperature are the same as in figure 6. Experimental points are taken from [11].

dielectric permittivities $\varepsilon_{11}(T,\sigma_{12})$ and $\varepsilon_{22}(T,\sigma_{12})$. The value of $\nu_a = \nu_1 - \nu_3 = 21$ K parameter, which describes the long-range interactions, is taken from [8] where the transverse properties of unstrained KD_2PO_4 crystals are studied. The value of $\psi_a = \psi_1 - \psi_2$ can be estimated from the relation

$$\psi_1 - \psi_2 < \frac{1}{\varepsilon_{12}} \left(\frac{T}{2} \frac{1 + bc_{12}}{a + \frac{b}{c_{12}}} - \nu_a \right).$$

In what follows $\psi_a = -12000$ K.

In figure 15 we show the stress and temperature dependences of $\varepsilon_{11}(T,\sigma_{12})$. Below the critical stress $\sigma_{12}(O)$ (curves $1' - 4'$) the temperature curves of the permittivity are qualitatively the same as at zero stress – with a jump at the ferroelectric phase transition. At the intermediate stresses $\sigma_{12}(O) < \sigma_{12} < \sigma_{12}^K$ (curves $5'$ and $6'$) the transverse permittivity has a downward jump at the transition from monoclinic to the paraelectric phase. At stresses above the critical one (curves $7'$ and $8'$) $\sigma_{12} > \sigma_{12}^K$ the permittivity $\varepsilon_{11}(T,\sigma_{12})$ is almost temperature independent. It is interesting that the magnitude of $\varepsilon_{11}(T,\sigma_{12})$ in the monoclinic phase is much greater than in the paraelectric or ferroelectric ones.

The other transverse permittivity $\varepsilon_{22}(T,\sigma_{12})$ has a similar temperature behaviour (see figure 16), except that it undergoes an upward jump at the transition from monoclinic to the paraelectric phase, and its magnitude in the monoclinic phase coincides with the low-temperature limit of $\varepsilon_{22}(T,\sigma_{12})$ in the ferroelectric phase – it is lower than in the paraelectric or ferroelectric phases.

As for the stress curves of both transverse permittivities, we can only say that this is perfectly well described by the above formulated rules; $\varepsilon_{11}(T,\sigma_{12})$ has upward jumps at the transitions between ferroelectric and paraelectric tetragonal phase II and I and between the tetragonal and monoclinic phases I and III. On the contrary,

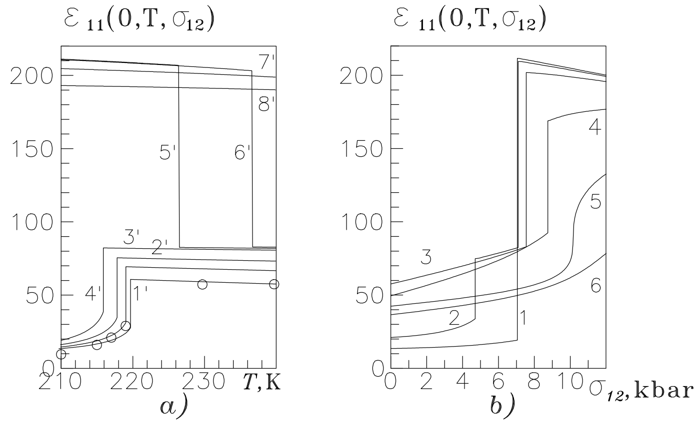

Figure 15. Dependences of the transverse dielectric permittivity $\varepsilon_{11}(T,\sigma_{12})$ on temperature at different stresses σ_{12} (a) and on σ_{12} (b) at different temperatures. Values of stress and temperature are the same as in figure 6. Experimental points are taken from [12].

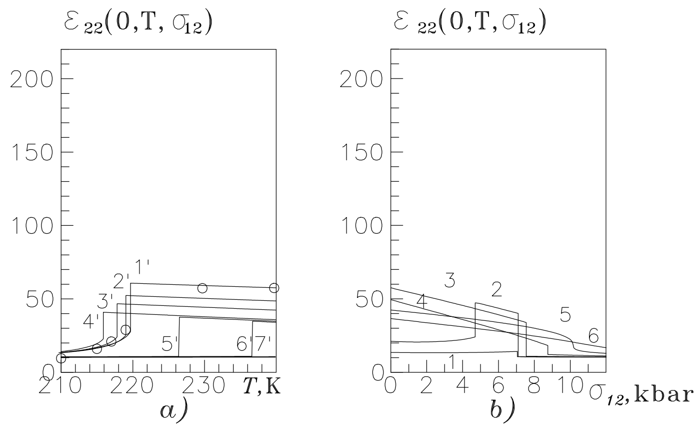

Figure 16. Dependences of the transverse dielectric permittivity $\varepsilon_{22}(T,\sigma_{12})$ on temperature at different stresses σ_{12} (a) and on σ_{12} (b) at different temperatures. Values of stress and temperature are the same as in figure 6. Experimental points are taken from [12].

$\varepsilon_{11}(T, \sigma_{12})$ has an upward jump at the transition between phases II and I and a downward jump at transition between the phases I and III.

References

1. Stasyuk I.V., Levitskii R.R., Zachek I.R., Moina A.P. The KD_2PO_4 ferroelectrics in external fields conjugate to the order parameter: Shear stress σ_6. // Phys. Rev B., 2000, vol. 62, No. 10, p. 6198–6207.
2. Stasyuk I.V., Levitskii R.R., Zachek I.R., Moina A.P., Duda A.S. The KD_2PO_4 ferroelectrics in external fields conjugate to the order parameter: Influence of shear stress σ_6 on the phase transition and physical properties of the KD_2PO_4 type ferroelectrics. // Journ. Phys. Studies, 2000, vol. 4., No. 2, p. 190–201 (in Ukrainian).
3. Stasyuk I.V., Biletskii I.N. Influence of omnidirectional and unaxial stress on the ferroelectric phase transition in crystals of KH_2PO_4 type. // Bull. Ac. Sci. USSR. Phys. Ser., 1983, vol. 4, No. 4., p. 79–82.
4. Stasyuk I.V., Biletskii I.N., Styahar O.N. Pressure induced phase transitions in the uniaxially strained ferroelectrics of KD_2PO_4-type. // Ukr. Phys. Journ., 1986, vol. 31, No. 3, p. 567–571. (in Russian)
5. Stasyuk I.V., Levitskii R.R., Moina A.P. External pressure influence on ferroelectrics and antiferroelectrics of the KH_2PO_4 family crystals: A unified model. // Phys. Rev. B., 1999, vol. 59, No. 13, p. 8530–8540.
6. Levitskii R.R., Zachek I.R., Mits I.Ye. Thermodynamics and longitudinal relaxation of ferroelectrics $K(H_{1-x}D_x)_2PO_4$. Preprint of Institute of Theoretical Physics, ITF–87–114R, Kiev, 1987, 48 p. (in Russian).
7. Levitskii R.R., Zachek I.R., Mits I.Ye. Transverse relaxation in $K(H_{1-x}D_x)_2PO_4$ type ferroelectrics. Preprint of Institute for theoretical Physics, ITF–87–115R, Kiev, 1987, 48 p. (in Russian)
8. Nelmes R.J. Structural studies of KDP and the KDP-type transition by neutron and X-ray diffraction: 1970–1985. // Ferroelectrics, 1987, vol. 71, p. 87–123.
9. Zwicker B., Helv.Phys.Acta 19, 523 (1946)
10. Shuvalov L.A., Mnatsakanyan A.V. The elastic properties of KD_2PO_4 crystals over a wide temperature range. // Sov. Phys. Crystall., 1996, vol. 11, p. 210–212
11. Chabin M., Giletta E. Polarisation and dielectric constant of KDP-type crystals. // Ferroelectrics, 1977, vol. 15, p. 149–154.
12. Volkova E.N. (private communication).

Вплив напруги $\sigma_1 - \sigma_2$ на фазовий перехід і фізичні властивості сегнетоелектриків типу KD_2PO_4

І.В.Стасюк [1], Р.Р.Левицький [1], І.Р.Зачек [2], А.С.Дуда [1]

[1] Інститут фізики конденсованих систем НАН України, 79011 Львів, вул. Свєнціцького, 1

[2] Державний університет "Львівська Політехніка", 79013 Львів, вул. С.Бандери, 12

Отримано 20 червня 2001 р.

На основі запропонованої раніше моделі вивчається вплив напруги $\sigma_1 - \sigma_2$ на сегнетоелектрики типу KD_2PO_4. В кластерному наближенні з врахуванням короткосяжних і далекосяжних взаємодій розраховано і досліджено пружні, діелектричні і п'єзоелектричні характеристики KD_2PO_4, проведено детальний числовий аналіз отриманих результатів. Досліджено температурні і баричні залежності розрахованих характеристик. Вивчаються індуковані напругою $\sigma_1 - \sigma_2$ фазові переходи.

PACS: *77.80.-e, 77.80.Bh, 77.84.Fa*

Ключові слова: *зсувна напруга, моноклінна фаза, фазова діаграма, п'єзоефект, деформація, KDP*